Critical length and time scales during the initial stages of nucleation in polymer blends

A. A. Lefebvre, J. H. Lee, and N. P. Balsara
Department of Chemical Engineering, University of California, Berkeley, California 94720

B. Hammouda
National Institute of Standards and Technology, Gaithersburg, Maryland 20899

(Received 1 October 2001; accepted 29 January 2002)

The initial stages of nucleation during liquid–liquid phase separation in polymer mixtures were studied by time-resolved small angle neutron scattering. The time required for nucleation vanishes exponentially as the stability limit (spinodal) is approached. The critical nucleus size decreases monotonically with increasing quench depth and remains finite at the spinodal. Our data differ qualitatively from theoretical predictions. © *2002 American Institute of Physics.*
[DOI: 10.1063/1.1463056]

Nucleation is a universal process for transforming a metastable phase into the stable equilibrium phase. Classical nucleation theory[1,2] and more recent extensions[3–7] provide a unified framework for describing diverse phenomena such as boiling, crystallization, condensation, magnetization, and liquid–liquid phase separation. In theory, these phase transitions are triggered by the formation of microscopic nuclei. Whether or not nucleation will occur in a given system hinges on the characteristics (size, fractal dimension, order parameter, etc.) of the smallest viable nucleus or the critical nucleus and the pathways available for its formation. In most systems, however, the subtle processes that lead to the formation of critical nuclei have escaped experimental scrutiny (e.g., Ref. 8). Consequently, we are not aware of any system wherein the experimentally determined characteristics of the initial stages of nucleation are compared with theory.

It has been recognized[9–11] that polymer systems are ideally suited for studying the kinetics of phase transitions. The large molecular size enables detection of small clusters of molecules using techniques such as small angle neutron scattering (SANS). In addition, kinetic processes are slow due to the entanglement of polymer chains and this enables time-resolved measurements. In a previous paper,[12] we demonstrated how these features could be exploited to investigate the initial stages of nucleation in a series of multicomponent polymer mixtures. Unfortunately, a direct comparison between theory and experiment was not possible because detailed theories of nucleation[1–7] are limited to binary systems. In this paper we present data obtained during the initial stages of nucleation in a binary polymer mixture. We compare theory and experiment with no adjustable parameters.

Partially deuterated polymethylbutylene (dPM) and hydrogenous polyethylbutylene (hPE) homopolymers were synthesized and characterized using methods described in Ref. 13. The polymers were purified by filtering through a 0.2 μm filter and precipitation. The numbers of repeat units per chain in the two components were determined to be $N_{hPE}=4260$, and $N_{dPM}=3357$ (based on a 100 Å^3 repeat unit which is the basis for all of the parameters reported here), the average number of deuterium atoms per repeat unit in dPM was 4.5. The radius of gyration (R_g) of both dPM and hPE chains were 16 ± 1 nm.[12] We prepared two binary blends, B1 and B2, with dPM volume fractions $\phi=0.161$ and 0.099, respectively. The blends were studied by time-resolved SANS on the NG3 beamline at the National Institute of Standards and Technology (NIST) in Gaithersburg, Maryland. One four-day experimental run was performed on blend B1, and two four-day experimental runs, using two different samples, were performed on blend B2. Data acquisition times for each SANS profile ranged from 2 to 30 min. We report the azimuthally averaged raw scattering intensity (without background correction), I, as a function of q [$q=4\pi\sin(\theta/2)/\lambda$, θ is the scattering angle, and λ, the wavelength of the incident neutrons, was 14 Å]. Separate experiments with analogous blends show that the smallest reported $I(q)$ is a factor of 15 larger than the background scattering (including empty cell and incoherent scattering). Details regarding instrument configuration and data reduction procedures are similar to our previous studies[12] and will be given in a full paper.[14]

The equilibrium thermodynamic properties of blends of the dPM and hPE polymers used in this study have been thoroughly investigated.[15] The temperature and pressure (T and P) dependence of the binodal and spinodal curves of blends B1 and B2, determined in Ref. 15, are shown in Fig. 1. Also shown in Fig. 1 are the T, P values where the phase separation kinetics were studied. The blends were homogenized at the start of each experiment by heating above the binodal temperature at atmospheric pressure (109 °C for B1 and 79 °C for B2). Homogenization was verified by ensuring that the SANS profiles measured at the end of the homogenization step were in quantitative agreement with theoretical predictions based on the random phase approximation and previously reported measurements.[15] We were able to perform multiple phase separation experiments on the same sample because homogenization of PM/PE blends is ex-

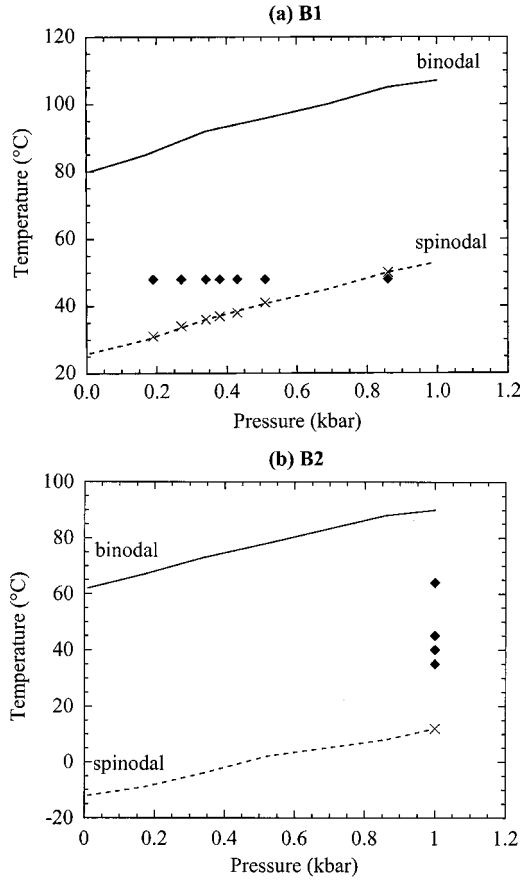

FIG. 1. Phase diagrams for blends (a) B1 and (b) B2 showing temperature (T) vs pressure (P) for binodal and spinodal curves taken from Ref. 15. The filled diamonds represent the locations where phase transition kinetics were studied. The crosses represent the location of the spinodal corresponding to each kinetic experiment.

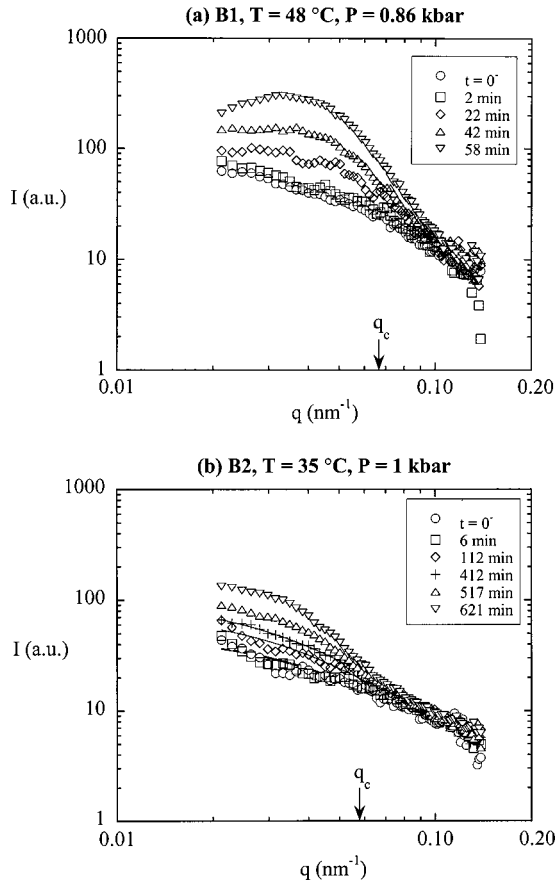

FIG. 2. Time dependence of the SANS intensity vs scattering vector q of blends (a) B1 at $T=48\,^{\circ}\mathrm{C}$, $P=0.86$ kbar, and (b) B2 at $T=35\,^{\circ}\mathrm{C}$ and $P=1$ kbar.

tremely rapid (requiring less than 10 min).[16] The homogenized blends were then cooled under isobaric conditions to the temperature of interest and then subjected to an isothermal pressure quench to obtain the desired T and P.

The SANS profiles were monitored throughout the entire quenching process. In all cases, no evidence of nucleation was observed prior to the pressure quench ($t=0^{-}$). We thus define time zero ($t=0$) as the time at which the pressure quench was initiated. Most of our quenches were located in the metastable region of the phase diagram, between the binodal and spinodal curves (Fig. 1). However, we did conduct one experiment inside the spinodal [Fig. 1(a)].

Typical SANS data obtained during the initial stages of phase separation are shown in Fig. 2. In Fig. 2(a) we show the data obtained from sample B1 inside the spinodal ($T=48\,^{\circ}\mathrm{C}$, $P=0.86$ kbar). We see relatively rapid phase separation and the development of a scattering peak at $q_{\mathrm{peak}}=0.035\ \mathrm{nm}^{-1}$. In contrast, no scattering peaks were obtained in any of the quenches located outside the spinodal. An example of such data is shown in Fig. 2(b) where we show data obtained from sample B2 at $P=1$ kbar at quench temperatures of $35\,^{\circ}\mathrm{C}$. All of the data obtained from the metastable systems were qualitatively similar to that shown in Fig. 2(b) except the shallowest quench ($T=64\,^{\circ}\mathrm{C}$) performed on blend B2 where no change in the SANS intensity was found up to $t=1000$ min. In the remainder of the paper, we focus on the deeper quenches where significant changes in the SANS profiles were recorded.

In the inset of Fig. 3, we show the time dependence of $I(q=0.021\ \mathrm{nm}^{-1})$ after quenching blend B2 to $T=35\,^{\circ}\mathrm{C}$, $P=1$ kbar [the same data set shown in Fig. 2(b)]. We see two dominant regimes: the nucleation stage ($t<450$ min) wherein the increase in I was slow and within experimental uncertainty, and the late stage ($t>450$ min) wherein I increases rapidly.[17] In systems with significant nucleation barriers, one expects a slow nucleation process followed by a rapid growth process. We define the nucleation time τ_{nucl} to be the time window within which the changes in I are comparable to experimental uncertainty (Fig. 3 inset). We determined τ_{nucl} for all of the quenches, and our results are shown in Fig. 3 where we show the quench depth dependence of τ_{nucl} for both samples, B1 and B2. The abscissa in Fig. 3 is χ/χ_s where χ is the Flory–Huggins interaction parameter at the T and P values at which the phase separation experiments were carried out and χ_s is the value of χ at the spinodal located by crosses in Fig. 1. The dependence of χ for dPM/hPE mixtures on T, P is given in Ref. 15. Figure 3 shows that the nucleation time decreases exponentially as the spinodal is approached. The results in Fig. 3 are in reasonable agreement with expectations because τ_{nucl} is related to the activation barrier that must be overcome by nucleation,

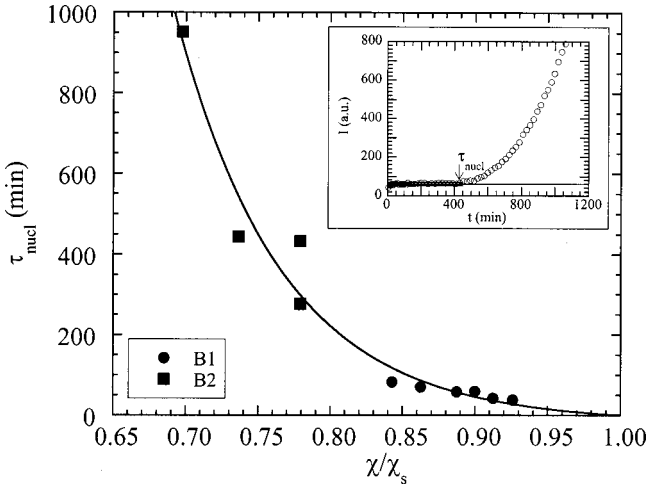

FIG. 3. The dependence of τ_{nucl} on quench depth χ/χ_s for blends B1 and B2. The curve is the least squares fit of the equation $\tau_{\mathrm{nucl}}/\tau_0 = \exp[-\mathrm{B}(\chi/\chi_s - 1)] - 1$ through the data which gives $\tau_0 = 16.2$ min and B $= 13.4$. Inset: Determination of the nucleation time τ_{nucl} of blend B2 at $T = 35\,^{\circ}\mathrm{C}$ and $P = 1$ kbar from the time dependence of the SANS intensity, $I(q = 0.021\ \mathrm{nm}^{-1})$, and the horizontal line shows the mean value of I for $t \leqslant \tau_{\mathrm{nucl}}$.

and this barrier is believed to vanish at the spinodal. The curve in Fig. 3 is the least squares fit of an empirical equation $\tau_{\mathrm{nucl}}/\tau_0 = \exp[-B(\chi/\chi_s - 1)] - 1$ through the data. The parameter B, which is 13.4 for our system, describes the quench depth dependence of the nucleation barrier.

More insight into the nucleation process is gained by examining the q-dependence of the SANS profiles (Fig. 2). To our knowledge, theoretical predictions for the structure factor during the initial stages of nucleation do not exist. Based on considerations given in Ref. 12, we used the Ornstein–Zernike (OZ) equation for analyzing the data obtained during the initial stages of nucleation ($t < \tau_{\mathrm{nucl}}$): $I(q) = I_0/[1 + q^2\xi^2]$. The curves in Fig. 2(b) are least squares OZ fits through the $0.02\ \mathrm{nm}^{-1} \leqslant q \leqslant 0.08\ \mathrm{nm}^{-1}$ data. In Figs. 4(a) and 4(b) we show the time dependence of I_0 and ξ, respectively, obtained at different quench depths. It is evident that a broad spectrum of behaviors is observed: Deep quenches lead to rapid changes in I_0 and ξ while shallow quenches lead to slow changes in I_0 and ξ. In Fig. 4(c) we plot I_0 versus ξ obtained at the same time t, normalized by the pre-quench values of these variables (at $t = 0^-$). In spite of the fact that the phase transition kinetics are strongly dependent on quench depth [see the dependence of τ_{nucl} on quench depth in Fig. 2(b) and the time dependencies of I_0 and ξ in Figs. 4(a) and 4(b)], we find that all of the data collapse when plotted in the format used in Fig. 4(c). This is expected if one assumes that the underlying mechanism for the phase transition is the same for all of the quenches shown in Fig. 4. Further, the observed scaling is not very different from $I_0 \sim \xi^{0.5}$. A least squares fit through the data gives $I_0 \sim \xi^{0.58 \pm 0.04}$ [line in Fig. 4(c)]. Since the observed scaling is similar to that expected from mean-field concentration fluctuations,[18] the data in Fig. 4 suggests that nucleation occurs homogeneously by the amplification of concentration fluctuations. Homogeneous nucleation is expected for deep quenches in the vicinity of the spinodal (Fig. 1). The main

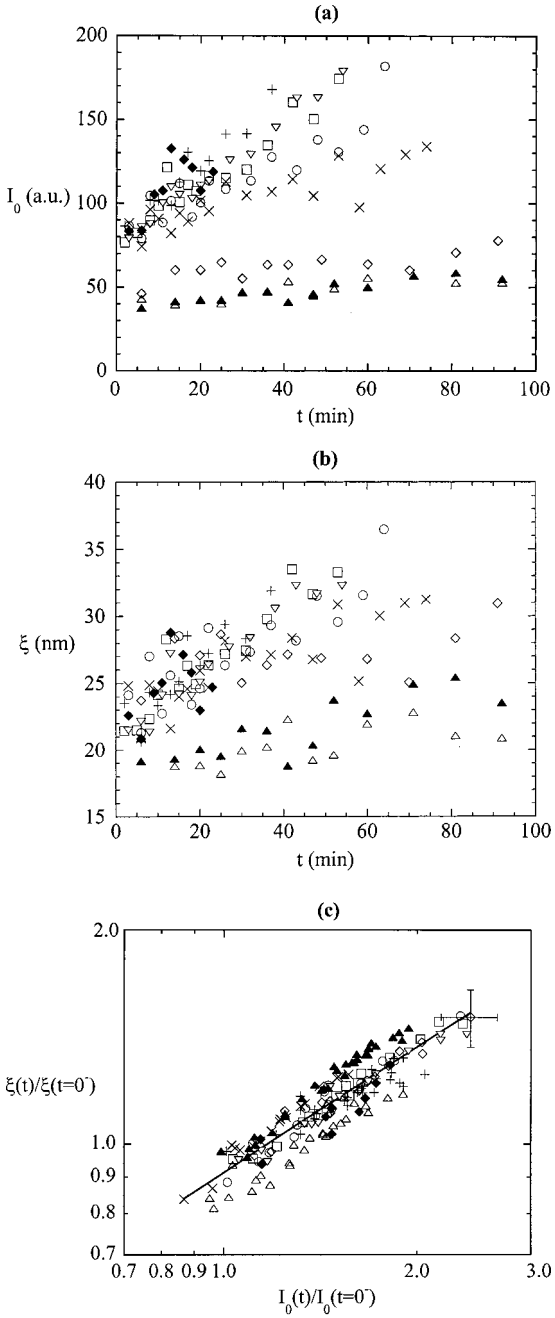

FIG. 4. The time dependence of the Ornstein–Zernike parameters during the early stages of nucleation. (a) I_0 vs t. (b) ξ vs t. (c) I_0 vs ξ, normalized by their pre-quench values. Sample B1-crosses: 0.19 kbar, circles: 0.27 kbar, squares: 0.34 kbar, upside down triangles: 0.38 kbar, open diamonds: 0.43 kbar, and solid diamonds: 0.51 kbar. Sample B2-solid triangles: 40 °C, and the pluses and open triangles: two separate 35 °C quenches. The line in (c) is the least-squares power law fit through the data. Error bars indicate average uncertainty in parameters.

characteristic that distinguishes homogeneous nucleation [Fig. 2(b)] from spinodal decomposition [Fig. 2(a)] is the absence of a dominant length scale, i.e., a scattering peak, during nucleation.

A common feature of all of the SANS profiles obtained during the early stages is that they merge at a critical scattering vector q_c (see arrows in Fig. 2); the SANS intensity at $q > q_c$ is independent of time during the early stage of phase separation. Since the formation of structures with a charac-

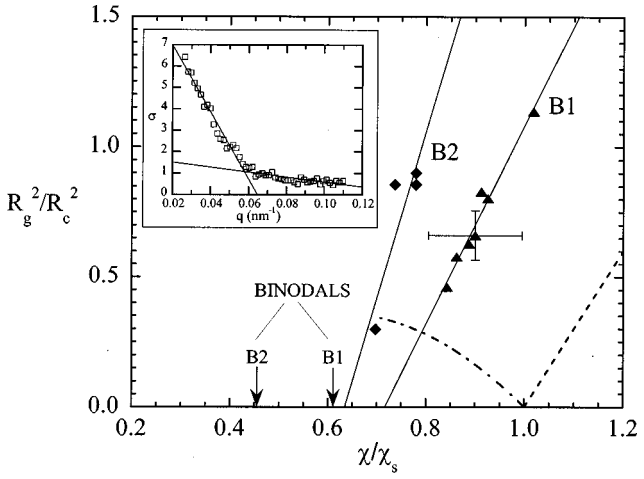

FIG. 5. A plot of $(R_g/R_c)^2$ vs quench depth χ/χ_s for blends B1 and B2, where R_g is the radius of gyration of the chains and R_c is the critical nucleus size. The solid lines are least squares fits through the data. The dashed lines are theoretical predictions [Eqs. (1) and (2)]. The theoretical curves for blends B1 and B2 in the nucleation regime are nearly indistinguishable in the range of interest (ordinate difference is less than 0.03). For simplicity, a single curve (the average of the two theoretical curves) is shown. Arrows indicate the value of χ/χ_s at the binodals of blends B1 and B2. Inset: σ (standard deviation of I) vs q for B2 quenched to $T=35\,^{\circ}\mathrm{C}$ and $P=1$ kbar with the two line least squares fit. Error bars indicate average uncertainty in parameters.

teristic length ξ will lead to an increase in scattering at scattering vectors $q\approx 1/\xi$, the lack of an increase in scattering in the range $q>q_c$ indicates the absence of growing structures with characteristic lengths smaller than $1/q_c$.[12] *The data thus suggest that the merging of the scattering profiles is a signature of the critical nucleus, and its size (ignoring prefactors)* $R_c=1/q_c$. The scaling law established in Fig. 4(c) indicates that the same prefactor applies to all of the quenches. While we do not suggest that our interpretation is unique, it is difficult to envision other physical processes that would lead to the observed changes in SANS.

We use the following procedure to determine the position of q_c. The change in the scattering intensity with time at each value of q is quantified by calculating $\sigma(q)$, the standard deviation of I in the time interval $t\leqslant\tau_{\mathrm{nucl}}$. Typical results are shown in the inset of Fig. 5. We used the two-line least squares fitting procedure, described in Ref. 12, to fit the σ versus q data and obtain the two lines shown in the Fig. 5 inset. The location of the intersection of the two lines gives q_c. In Fig. 5 we show the dependence of the critical length scale on quench depth by plotting $(R_g/R_c)^2$ versus χ/χ_s. It is evident that τ_{nucl}, for both blends depends only on χ/χ_s (Fig. 3), whereas R_g^2/R_c^2 depends both on χ/χ_s and ϕ (Fig. 5). Also shown in Fig. 5 are theoretical predictions for $(R_g/R_c)^2$ for the mean field theory of polymer blends:[3,19,20]

$$\left(\frac{R_g}{R_c}\right)^2=\left(\frac{2\chi N}{0.73}\right)^2\phi(1-\phi)\left(\frac{1}{2}-\frac{1}{2}\sqrt{1-\frac{2}{\chi N}}-\phi\right)\times\left(\sqrt{1-\frac{2}{\chi N}}\right)\quad(\chi/\chi_s<1,\ \text{i.e., nucleation})\qquad(1)$$

$$\left(\frac{R_g}{R_c}\right)^2=3\left(\frac{\chi}{\chi_s}-1\right)\quad(\chi/\chi_s>1,\ \text{i.e., spinodal decomposition}).\qquad(2)$$

Equation (1) only applies for deep quenches near the spinodal.[3]

As shown in Fig. 5, the mean-field theory of phase separation[3] predicts an *increase* in R_c with increasing quench depth in the nucleation regime ($\chi/\chi_s=1$) ending in a divergence of R_c at the spinodal. In contrast, the experimentally determined R_c values in Fig. 5 *decrease* with increasing quench depth. The solid lines, in Fig. 5, are least-squares linear fits through the data. Extrapolations of the data suggest a divergence of R_c at χ/χ_s values of 0.72 and 0.63 for blends B1 and B2 respectively. These values are well removed from the divergence anticipated by the mean-field theory at $\chi/\chi_s=1$. The experimentally determined points of divergence lie roughly halfway between the binodal and spinodal points (Fig. 5). The nucleation mechanism that we have identified thus appears to have a limited range of applicability ($0.72<\chi/\chi_s<1$ for B1 and $0.63<\chi/\chi_s<1$ for B2). Note that our experiment on blend B2 at $\chi/\chi_s=0.57$ [shallowest quench in Fig. 1(b)] showed no evidence of nucleation in the 1000 min experimental window. Thus nucleation at shallow quench depths ($\chi/\chi_s<0.72$ for B1 and $\chi/\chi_s<0.63$ for B2) is triggered by processes with different characteristic length and time scales than those that we have identified.

In summary, we have studied nucleation in a binary polymer mixture. Systematic studies of nucleation are often thwarted by the overwhelming role of uncontrolled foreign objects like dust and defects in container walls. It appears that such problems have been circumvented in our experiments because of the chemical similarity of the blend components: both components are long alkanes and thus there is no significant preferential affinity for typical uncontrolled foreign objects. This enables measurement of the quench depth dependence of the critical length and time scales involved in nucleation. Many aspects of our data are qualitatively inconsistent with current theories. In particular, we find that the length scale of the nucleating entities do not increase (or diverge) as the spinodal is approached. We hope that our results will guide the development of a quantitative understanding of the initial stages of nucleation.

The authors thank K. Binder for educational discussions and the National Science Foundation (Grant No. CTS-0196066) for financial support. The SANS instrument is supported by Grant No. DMR-9986442 from the National Science Foundation to NIST.[21]

[1] J. W. Gibbs, *The Scientific Papers of J. Willard Gibbs* (Dover, New York, 1961).
[2] R. Becker and W. Doring, Ann. Phys. (Leipzig) **24**, 719 (1935).
[3] J. W. Cahn and J. E. Hilliard, J. Chem. Phys. **31**, 688 (1959).
[4] K. Binder and D. Stauffer, Adv. Phys. **25**, 343 (1976).
[5] K. Binder, Phys. Rev. A **29**, 341 (1984).
[6] J. S. Langer and A. J. Schwartz, Phys. Rev. A **21**, 948 (1980).
[7] D. W. Heerman and W. Klein, Phys. Rev. B **27**, 1732 (1983).
[8] S. Krishnamurty and W. I. Goldburg, Phys. Rev. A **22**, 2147 (1980).
[9] M. Okada and C. C. Han, J. Chem. Phys. **85**, 5317 (1986).
[10] F. S. Bates and P. Wiltzius, J. Chem. Phys. **91**, 3258 (1991).

[11] H. Jinnai, H. Hasegawa, T. Hashimoto, and C. C. Han, J. Chem. Phys. **99**, 4845 (1993).
[12] A. A. Lefebvre, J. H. Lee, H. S. Jeon, N. P. Balsara, and B. Hammouda, J. Chem. Phys. **111**, 6082 (1999).
[13] N. P. Balsara, S. V. Jonnalagadda, C. C. Lin, C. C. Han, and R. Krishnamoorti, J. Chem. Phys. **99**, 10011 (1993).
[14] A. A. Lefebvre *et al.* (unpublished).
[15] A. A. Lefebvre, J. H. Lee, N. P. Balsara, and B. Hammouda, Macromolecules **33**, 7977 (2000).
[16] B. Hammouda, N. P. Balsara, and A. A. Lefebvre, Macromolecules **30**, 5572 (1997).
[17] At very early times (e.g., $t<15$ in Fig. 3, inset) an extremely rapid rise in I is seen; similar data were presented in Ref. 12. This is attributed to the response of concentration fluctuations to the change in pressure.
[18] P. G. de Gennes, *Scaling Concepts in Polymer Physics* (Cornell UniversityPress, Ithaca, 1979).
[19] J. W. Cahn, Trans. Am. Inst. Min., Metall. Pet. Eng. **242**, 166 (1968).
[20] Equations (1) and (2) apply to a blend of polymers with the same N_i and R_g. In our blends R_g is the same (16 ± 1 nm) but N_i are different. We take N to be the average value of N_i (3809 at atmospheric pressure and temperature) in our comparisons of theory and experiment.
[21] Identification of equipment and materials does not imply recommendation by the National Institute of Standards and Technology.